Metaweaves: Sector-Way Nonreciprocal Metasurfaces

Y. Mazor and Ben Z. Steinberg*

School of Electrical Engineering, Tel Aviv University, Ramat-Aviv, Tel-Aviv 69978, Israel

(Received 10 October 2013; revised manuscript received 17 March 2014; published 18 April 2014)

Confluent with the single dimension of time, breach of time-reversal symmetry is usually perceived as a one-dimensional concept. In its ultimate realization—the one-way guiding device—it allows optical propagation in one direction, say $+z$, and forbids it in the opposite direction $-z$. Hence, in studies of time-reversal asymmetry the mapping $t \mapsto -t$ is naturally associated with $z \mapsto -z$. However, strongly nonreciprocal or one-way nanoscale threads can be used to weave metasurfaces thus adding dimensions to this concept. In this new family of surfaces the aforementioned association cannot be made. An example of appropriate threads is the planar one-way particle chains based on the two-type rotation principle. The resulting surfaces—the metaweaves—possess generalized nonreciprocity such as "sector-way" propagation, and offer new possibilities for controlling light in thin surfaces. We study several metaweave designs and their asymmetries in the wave-vector space.

DOI: 10.1103/PhysRevLett.112.153901 PACS numbers: 41.20.Jb, 42.70.Qs, 42.82.Et, 78.67.Bf

Strongly nonreciprocal structures and one-way propagation schemes have attracted considerable attention in the last decade. Numerous different configurations were suggested to create one-way structures; most of them share a common concept. First, one violates Lorentz's reciprocity, either by making the susceptibility χ asymmetric using magnetization or by time modulation of χ. Hence, propagation in opposing directions possesses different sets of features. Then, another mechanism (e.g., geometric) is employed to make one set preferable, yielding one-way behavior. One-way total reflection from infinite periodic magneto-optical (MO) layers was demonstrated in Ref. [1]. In other configurations, one-way behavior exists at the interface between two photonic crystals (PhCs), or between a PhC and a metal, where at least one of them consists of MO or gyromagnetic material [2–8]. Photonic topological insulators based on edge states between two bianisotropic metamaterials were suggested in Ref. [9]. In all these schemes the one-way edge states are assumed to be completely separated from the surrounding free space by the semi-infinite supposedly impenetrable structures on both sides. One-way transmission through a screen assembly composed of a perforated perfect electric conductor placed at the interface of a MO medium is shown in Ref. [10]. Likewise, one-way transmission through combined screens of MO material and ϵ-near-zero material [11], through combined screens of MO and negative-ϵ materials [12], or through a screen of magnetized ϵ-near-zero material in a Voigt configuration [13], were suggested. Nonmagnetic one-way behavior was achieved by time-modulation of ϵ [14,15]. In all the schemes above, the transverse dimensions of the one-way structure must be of several wavelengths (or several PhC periods) to operate properly.

One-way guiding structures consisting of a single linear chain of nanoscale plasmonic particles were suggested in Refs. [16–19]. These studies include analytical models based on the discrete dipole approximation (DDA), and full-wave simulations with material loss and finite particle size verifying the one-way property for realistic parameters. The underlying physics is based on the interplay of two types of rotations: geometric and electromagnetic. An example is shown in Fig. 1(a). A chain of plasmonic particles supporting trapped plasmonic modes is exposed to transverse magnetization $\boldsymbol{B}_0 = \hat{z}B_0$. $\boldsymbol{B}_0$ induces longitudinal rotation of the chain modes: the excited dipole in

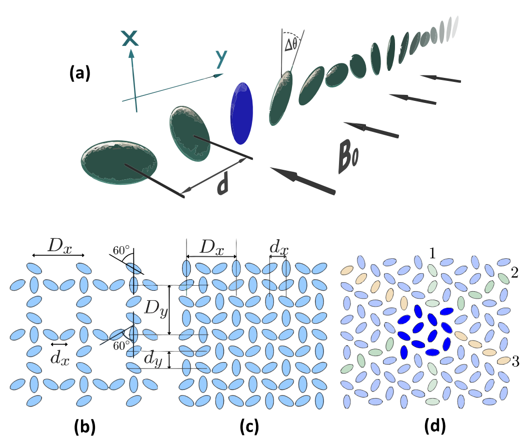

FIG. 1 (color online). A basic one-way thread that can be used to weave surfaces, and our metaweaves. (a) A planar chain of plasmonic ellipsoids with transverse magnetization and longitudinal chirality, supporting one-way guiding. (b)–(d) Some optional weaves, subject to a bias magnetization $\boldsymbol{B}_0 = \hat{z}B_0$. (b) A "snug" rectangular weave of two identical chains with $\Delta\theta = 60°$ ($D_x = D_y = 3d$). (c) A tight rectangular weave of the same chains. (d) A tight hexagonal weave of any two of the three chains with $\Delta\theta_{1,2,3} = 60°, 75°, 15°$. The rectangular period is marked by dark ellipsoids.

each particle rotates in the (x, y) plane. Then, a longitudinal chirality is introduced by using nonspherical particles that rotate in the (x, y) plane, with rotation step $\Delta\theta$, as shown in the figure. Two-type rotations coexist in a single plane, and their interplay enhances nonreciprocity and creates one-way guiding [17]. This structure has several appealing properties: (a) It possesses nanoscale transverse size. (b) Propagation in the "forbidden" direction decays by 2 orders of magnitude over distances of $O(\lambda)$. (c) B_0 is weaker than other magnetization-based approaches. (d) Since both rotations take place in a single plane coinciding with the chain axis, particle dimension in the $\hat{z}$ direction is unimportant; one may use flat ellipsoidal flakes. Hence, the structure is flat, amenable to planar fabrication.

The purpose of the present work is to generalize the one-dimensional concept of broken time-reversal symmetry, by suggesting the metaweaves. Being a nanoscale wide, flat, one-way "thread," the longitudinal-chirality chain in Fig. 1(a) may be used to "weave" metasurfaces that add dimensions to the concept of broken time-reversal symmetry. In these structures the natural association of the 1D mapping $t \mapsto -t$ with the 1D mapping $z \mapsto -z$, so commonly used in studies of time-reversal asymmetry, cannot be made. Rather, the former needs to be associated with a higher dimensional mapping in the plane. To characterize this association and the ensuing optical behavior we define the notion of sector-way propagation; a structure is said to be ϕ sector-way if, when excited by a point source, it allows propagation only into a cone whose vertex angle is ϕ. Our metaweaves possess sector-way propagation dynamics and offer new possibilities for controlling the flow of light in a plane.

There are many ways to weave a surface. Some examples are shown in Figs. 1(b)–1(d). The most natural choice is the "snug" weave, defined as the case where the weave period (= interthread distance) matches the chain period. The "tight" weave is defined as the case when the interchain distance is the same as the interparticle distance within the corresponding single chain. The weave periods in the $\hat{\boldsymbol{x}}, \hat{\boldsymbol{y}}$ directions D_x, D_y for the snug and tight weaves coincide with the corresponding chains period.

Due to interthreads coupling, the metaweave properties may not always be inferred by a mere "product" of the single threads. Nevertheless, sector-way propagation is observed even in tight weaves, reflecting the robust nature of the two-type rotation principle and its compatibility for multidimensional nonreciprocity.

Our weaves are systematically structured as follows. All particles possess the same shape, differing only by rotation. The m, n lattice location $\boldsymbol{r}_{m,n}$ and rotation $\theta_{m,n}$, are given by

$$\boldsymbol{r}_{m,n} = m\boldsymbol{a}_1 + n\boldsymbol{a}_2, \tag{1}$$

$$\theta_{m,n} = m\Delta\theta_1 + n\Delta\theta_2. \tag{2}$$

Here $\boldsymbol{a}_1, \boldsymbol{a}_2$ are the fundamental lattice vectors along which the chains are weaved, and $\Delta\theta_{1,2}$ are the corresponding rotation steps. In tight weaves all lattice points are occupied by a particle, but every nontight weave possesses empty points. We denote by $\mathbb{P}$ the set of all occupied points.

We use the DDA to study our metaweaves. Under the DDA, a particle response to an exciting local field $\boldsymbol{E}^L$ (the field at the particle's location, in the absence of the particle), is described by its dipole moment $\boldsymbol{p} = \boldsymbol{\alpha}\boldsymbol{E}^L$, where $\boldsymbol{\alpha}$ is the particle polarizability matrix. It formally holds when the particle size D_p is much smaller than λ and when the interparticle distance $d \gg D_p$. However, studies show excellent agreement with exact solutions even when $d = 1.5D_p$ [20]. Also, full wave simulations with finite particle size and material loss show that the one-way chains dynamics is predicted well by the DDA [17,18]. Note that $\boldsymbol{B}_0$ affects only the xy, yx entries of $\boldsymbol{\alpha}$. Hence, the z components of $\boldsymbol{\alpha}$ can be ignored, rendering $\boldsymbol{\alpha}$ a 2×2 matrix, and $\boldsymbol{p}$ a two-element vector. In our weaves, the m, n particle polarizability $\boldsymbol{\alpha}_{m,n}$ is

$$\boldsymbol{\alpha}_{m,n} = \mathbf{T}_{-\theta_{m,n}}\boldsymbol{\alpha}\mathbf{T}_{\theta_{m,n}}, \tag{3}$$

where $\mathbf{T}_\theta$ is a rotation by θ operator in the (x, y) plane, and $\boldsymbol{\alpha}$ is the polarizability of a reference ellipsoidal particle. A Drude-model $\boldsymbol{\alpha}$ of a magnetized ellipsoid that takes into account the particle's radiation loss is used here (see, e.g., Ref. [17]). We assume lossless material. It has been shown that material loss does not change essentially the one-way thread properties if one uses much denser chains, but in this case valid modeling requires full-wave simulations [17]. For our structures this is beyond currently available computing power. With the definitions above, the surface modes are governed by the difference equation

$$\boldsymbol{p}_{\boldsymbol{m}} = \boldsymbol{\alpha}_{\boldsymbol{m}} \sum_{\boldsymbol{m}' \in \mathbb{P}_{\boldsymbol{m}}} \mathbf{G}(\boldsymbol{r}_{\boldsymbol{m}}, \boldsymbol{r}_{\boldsymbol{m}'})\boldsymbol{p}_{\boldsymbol{m}'}, \boldsymbol{m} \in \mathbb{P}, \tag{4}$$

where $\boldsymbol{m}$ ($\boldsymbol{m}'$) denotes the integers pair m, n (m', n'). $\mathbf{G}(\boldsymbol{r}, \boldsymbol{r}')$ is the dyadic Green's function [21]; hence, $\mathbf{G}(\boldsymbol{r}, \boldsymbol{r}')\boldsymbol{p}$ gives the electric field at $\boldsymbol{r}$ due to a dipole $\boldsymbol{p}$ at $\boldsymbol{r}'$. The set $\mathbb{P}_{\boldsymbol{m}}$ is the set $\mathbb{P}$ excluding the point $\boldsymbol{m}$.

The eigensolutions of Eq. (4) constitute the surface modes (i.e., in-plane propagation). This equation can be reduced to a finite matrix by exploiting the weave periodicity. We find that using the rectangular periodicity is the most convenient and efficient approach even for hexagonal weaves, mainly because symmetry-based k-space reductions (e.g., irreducible Brillouin zone) cannot be applied due to loss of reciprocity. For example, the parallelogram period of the lattice in Fig. 1(d) obtained from the hexagonal lattice vectors consists of 36 particles, while the rectangular periodicity cell consists of only 12 particles. Hence, we define $\mathbb{P}^0$ as the restriction of $\mathbb{P}$ to a reference rectangular period containing the origin. $\mathbb{P}^0$ consists of M

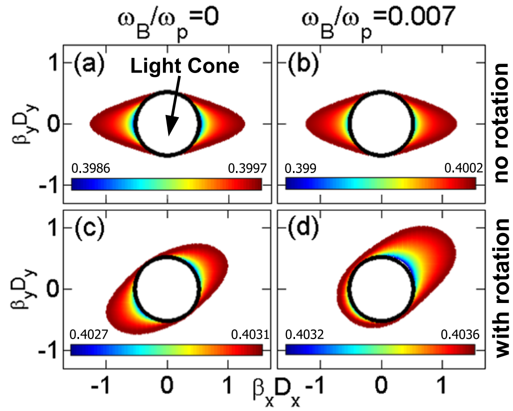

FIG. 2 (color online). Dispersion surfaces color coded according to frequency in units of ω/ω_p. (a) A weave with $\Delta\theta_{1,2} = 0$ and $B_0 = 0$. (b) $\Delta\theta_{1,2} = 0$, $B_0 \neq 0$. (c) $\Delta\theta_{1,2} = 60°$, $B_0 = 0$. (d) $\Delta\theta_{1,2} = 60°$, $B_0 \neq 0$.

particle locations $\boldsymbol{r}_1, \ldots, \boldsymbol{r}_M$, with the corresponding M polarizabilities $\boldsymbol{\alpha}_1, \ldots, \boldsymbol{\alpha}_M$ [Eq. (3) consists of at most M different $\boldsymbol{\alpha}_{m,n}$'s]. Each point $\boldsymbol{m} \in \mathbb{P}$ can be expressed by the three integers m, ℓ_x, ℓ_y where $m \in \{1, \ldots, M\}$ counts the points in $\mathbb{P}^0$, and ℓ_x, ℓ_y count the unit cells. By periodicity, the dipole response in each particle $\boldsymbol{p}_{m,(\ell_x,\ell_y)}$ satisfies

$$\boldsymbol{p}_{m,(\ell_x,\ell_y)} = \boldsymbol{p}_m e^{i\beta\cdot\boldsymbol{D}_{\ell_x,\ell_y}}, \tag{5}$$

where $\beta = \hat{\boldsymbol{x}}\beta_x + \hat{\boldsymbol{y}}\beta_y$ is the wave vector, and $\boldsymbol{D}_{\ell_x,\ell_y} = \hat{\boldsymbol{x}}\ell_x D_x + \hat{\boldsymbol{y}}\ell_y D_y$. Using the above expression in Eq. (4), we obtain a matrix equation with $M \times M$ blocks of 2×2 submatrices, governing the M vectors $\boldsymbol{p}_m$,

$$(\boldsymbol{\alpha}_m^{-1} - \boldsymbol{S}_{m,m})\boldsymbol{p}_m - \sum_{\substack{n=1 \\ n\neq m}}^{M} \boldsymbol{S}_{m,n}\, \boldsymbol{p}_n = \boldsymbol{0}, \tag{6}$$

where $\boldsymbol{S}_{m,n}$ are the 2×2 matrices

$$\boldsymbol{S}_{m,n} = {\sum_{\ell_x,\ell_y}}' \mathbf{G}(\boldsymbol{r}_m, \boldsymbol{r}_n + \boldsymbol{D}_{\ell_x,\ell_y}) e^{i\beta\cdot\boldsymbol{D}_{\ell_x,\ell_y}} \tag{7}$$

and where the ℓ_x, ℓ_y summation is over all integers. The prime indicates that the summation excludes the singular self-term arising in $\boldsymbol{S}_{m,m}$ when $\ell_x = \ell_y = 0$. This summation converges poorly, but it can be accelerated using the Ewald method [22,23], modified to account the self term exclusion [24]. The dispersion $\omega(\beta_x D_x, \beta_y D_y)$ is obtained numerically by nullifying the corresponding determinant. Since our metaweaves are non-Bravais lattices there are M dispersion surfaces for each of the particle's resonances, which need to be searched.

We turn now to some examples, starting with the snug rectangular weave of Fig. 1(b). The parameters are $d_x = d_y = \lambda_p/14.5$ ($\lambda_p = 2\pi c/\omega_p$). The particle's axis ratios

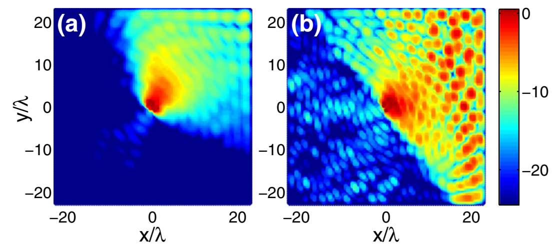

FIG. 3 (color online). The response $|\boldsymbol{p}_{m,n}|$ in dB of the snug weave of Figs. 1(b) and 2(d), to a dipole at the origin. (a) $\sim\pi/2$ sector-way guiding at $\omega = 0.40343\omega_p$. For Cu parameters, this sector-way is preserved over a bandwidth of more than 100 GHz. (b) $\sim\pi$ sector-way at $\omega = 0.40355\omega_p$.

are $a_x : a_y : a_z = 1 : 0.9 : 0.25$, where $a_x = d_x/4$. With these parameters the DDA is highly accurate. For Cu ($\lambda_p = 142$ nm) particles the diameter is $2a_x \approx 5$ nm and $d \approx 10$ nm (for larger Cu particles see the last example). Also $\Delta\theta = 60°$, and $\omega_b = -eB_0/m_e = 7 \times 10^{-3}\omega_p$ denotes magnetization strength (cyclotron frequency). The particle possesses two resonances (associated with a_x and a_y), and there are $M = 5$ particles in a period. Hence, we have ten dispersion surfaces, only some of which support sector-way guiding. An example is shown in Fig. 2. It is seen that symmetry under the operation $(\beta_x D_x, \beta_y D_y) \mapsto -(\beta_x D_x, \beta_y D_y)$ is broken when rotation and magnetization are simultaneously introduced. This strong asymmetry leads to "sector-way" guiding, explained as follows. There is a well-established theory of these one-way threads [19], showing that the excitation magnitude of a thread mode near the light-cone scales as

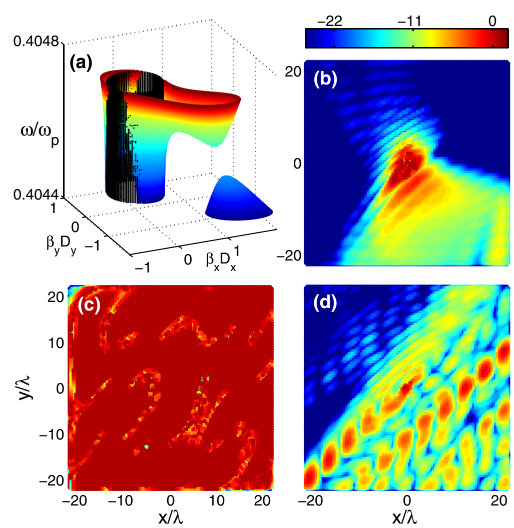

FIG. 4 (color online). (a) Another dispersion surface of the snug weave of Fig. 1(b). The light cone is shown by the black cylinder in the center. (b)–(d) Responses, (b) at $\omega = 0.404585\omega_p$ possessing $\pi/2$ sector-way guiding, (c) at $\omega = 0.40463\omega_p$ possessing "all-way" guiding, and (d) at $\omega = 0.404695\omega_p$ possessing π-way guiding.

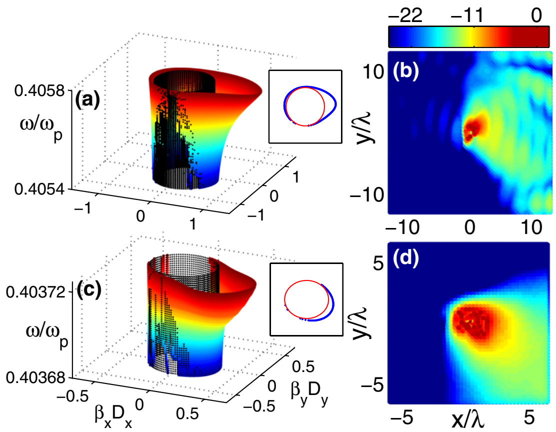

FIG. 5 (color online). Dispersion and response of the tight rectangular and hexagonal weaves of Fig. 1(c)–1(d). (a) Dispersion surface of the tight rectangular weave. (b) Sector-way response at $\omega = 0.40561\omega_p$. (c) Dispersion surface of the tight hexagonal weave. (d) Sector-way response at $\omega = 0.403685\omega_p$. The insets show the corresponding dispersion contours.

$$A = \frac{1-x}{\ln(1-x)}, \qquad x = |\beta|/k_0. \tag{8}$$

Hence, modes touching or residing very close to the light cone are practically nonexcitable. Figure 2(d) shows that the dispersion contours within the blue to green range, touch or nearly touch the light cone in the third quadrant; the normalized distance $1 - x \ll 0.05$. Hence, Eq. (8) predicts a reduction of more than 2 orders of magnitude in the corresponding modes excitation. Therefore, propagation in these directions (given by the dispersion's local gradient) is practically blocked. Figure 3 shows the response of this weave to an excitation of a unit dipole at its center. A $\pi/2$ and a π sector-way propagation are seen. The latter picture exhibits much stronger oscillations, because in the $\pi/2$ sector, most of the reflections occurring at the surface edge are in "forbidden" directions; hence, they decay exponentially as they leak energy to the free space. In comparison, in the π sector-way case some reflections occur at allowed directions and interfere with the modes propagating towards the edge.

Figure 4 shows another surface of the same weave, and a response to a dipole excitation at three different frequencies. $\pi/2$ sector-way, π sector-way, and "all-way" are observed. The sector-way shown in Fig. 4(b) is not obtained by an obvious "cartezian product" of the individual threads. Such a product would predict a sector that coincides with one of the plane quadrants, while the sector obtained is centered approximately around $-\hat{\boldsymbol{y}} + 0.3\hat{\boldsymbol{x}}, y < 0$. The high intensity saturated field in Fig. 4(c) is due to the fact that reflections at edges are all into allowed directions; hence, they fill the surface and increase the intensity. Now to the tight weaves. Figures 5(a) and 5(b) show the dispersion and the response of the tight rectangular weave of Fig. 1(c) with the same

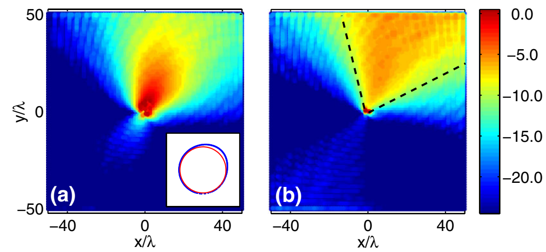

FIG. 6 (color online). Response of the snug rectangular weave of Fig. 1(b), using larger particles. The inset shows the corresponding dispersion contour. Here $\omega = 0.3988\omega_p$ ($\approx$820 THz for Cu). (a) Dipole response $|\boldsymbol{p}_{mn}|$. This sector-way is essentially preserved over $\approx$0.8 THz bandwidth. (b) $\sqrt{r}|\boldsymbol{p}_{mn}|$, i.e., the same response, but without the geometrical spreading effect. Along the dashed lines the intensity is reduced by e^{-2}.

parameters as above. Figures 5(c) and 5(d) show the dispersion and the response of the tight hexagonal weave of Fig. 1(d) with interparticle distance $d = \lambda_p/30$, with $a_x : a_y : a_z = 1:0.9:0.25$ where $a_x = d/4$, and with the same magnetization as above. Sector-way propagation is observed in both weaves.

As a last example, Fig. 6 shows the response of the snug rectangular weave of Fig. 1(b), using larger Cu particles with $2a_x = 16$ nm and the same axis ratios as before. Here $d = 24$ nm. Sector-way is observed. Finally, to get a better feeling of the nature of the metaweave trapped modes, Fig. 6(b) shows the same solution but multiplied by $r^{1/2}$ where r is the distance from the source at the center. This clears out a $r^{-1/2}$ decay due to 2D geometrical spreading. It is seen that now there is no decay at all along the sector central line. The same behavior applies to all the previous examples.

To conclude, a new family of metasurfaces, the metaweaves, was suggested and studied. These metaweaves are made of strongly nonreciprocal or one-way threads based on the two-type rotation principle. It has been shown that they suggest a systematic generalization of the one-dimensional concept of broken time-reversal symmetry, and its extension to higher dimensions. The result is a surface that exhibits sector-way guiding features that may offer new ways to control the flow of light in thin surfaces.

This research was supported by the Israel Science Foundation (Grant No. 1503/10).

*Corresponding author.
steinber@eng.tau.ac.il

[1] Z. Yu, Z. Wang, and S. Fan, Appl. Phys. Lett. **90**, 121133 (2007).
[2] F. D. M. Haldane and S. Raghu, Phys. Rev. Lett. **100**, 013904 (2008).
[3] S. Raghu and F. D. M. Haldane, Phys. Rev. A **78**, 033834 (2008).

[4] Z. Wang, Y. D. Chong, J. D. Joannopoulos, and M. Soljacic, Phys. Rev. Lett. **100**, 013905 (2008).
[5] Z. Yu, G. Veronis, Z. Wang, and S. Fan, Phys. Rev. Lett. **100**, 023902 (2008).
[6] Z. Wang, Y. D. Chong, J. D. Joannopoulos, and M. Soljacic, Nature (London) **461**, 772 (2009).
[7] K. Fang, Z. Yu, and S. Fan, Phys. Rev. B **84**, 075477 (2011).
[8] A. A. Asatryan, L. C. Botten, K. Fang, S. Fan, and R. C. McPhedran, Phys. Rev. B **88**, 035127 (2013).
[9] A. B. Khanikaev, S. H. Mousavi, W. K. Tse, M. Karagarian, A. H. MacDonald, and G. Shvets, Nat. Mater. **12**, 233 (2013).
[10] A. B. Khanikaev, S. H. Mousavi, G. Shvets, and Y. S. Kivshar, Phys. Rev. Lett. **105**, 126804 (2010).
[11] A. R. Davoyan, A. M. Mahmoud, and N. Engheta, Opt. Express **21**, 3279 (2013).
[12] M. Moccia, G. Castaldi, V. Galdi, A. Alu, and N. Engheta, arXiv:1308.3845v3.
[13] A. R. Davoyan and N. Engheta, arXiv:1309.2650v1.
[14] Z. Yu and S. Fan, Nat. Photonics **3**, 91 (2009).
[15] H. Lira, Z. Yu, S. Fan, and M. Lipson, Phys. Rev. Lett. **109**, 033901 (2012).
[16] Y. Hadad and B. Z. Steinberg, Phys. Rev. Lett. **105**, 233904 (2010).
[17] Y. Mazor and B. Z. Steinberg, Phys. Rev. B **86**, 045120 (2012).
[18] Y. Hadad and B. Z. Steinberg, Opt. Express **21**, A77 (2013).
[19] Y. Hadad, Y. Mazor, and B. Z. Steinberg, Phys. Rev. B **87**, 035130 (2013).
[20] S. A. Maier, P. G. Kik, and H. A. Atwater, Phys. Rev. B **67**, 205402 (2003).
[21] J. D. Jackson, *Classical Electrodynamics* (Wiley, New York, 1999), 3rd ed.
[22] P. P. Ewald, Ann. Phys. (Berlin) **369**, 253 (1921).
[23] K. E. Jordan, G. R. Richter, and P. Sheng, J. Comput. Phys. **63**, 222 (1986).
[24] S. Steshenko, F. Capolino, P. Alitalo, and S. Tretyakov, Phys. Rev. E **84**, 016607 (2011).